Journal of Applied Polymer Science

Evaluation of mechanical properties of Al_2O_3 and TiO_2 nano filled enhanced glass fiber reinforced polymer composites

Ramesh Kumar Nayak,[1] K. K. Mahato,[2] B. C. Routara,[1] Bankim Chandra Ray[2]

[1]School of Mechanical Engineering, KIIT University, Bhubaneswar, India

[2]Metallurgical and Materials Engineering Department, National Institute of Technology, Rourkela, India

Correspondence to: R. K. Nayak (E-mail: rnayakfme@kiit.ac.in)

ABSTRACT: The present investigation has emphasized the implication of nano fillers (Al_2O_3 and TiO_2) combined additions in glass fiber reinforced polymer composite on the variation of interlaminar shear strength (ILSS). The experiment has also investigated the effect of crosshead speed during testing and subsequent fracture surface analysis to find out the possible failure modes by scanning electron micrograph examinations. Loss and storage modulus have been experimentally evaluated to support the new findings in the present experimental design. It has been observed that the concurrent presence of nano Al_2O_3 and TiO_2 fillers improves the ILSS. Dynamic mechanical thermal analysis indicated that, the addition of nano fillers reduces the storage and loss modulus of the composites. However, glass transition temperature has not been altered by the nano fillers addition. Box–Behnken design of experiment of surface response methodology has been adopted to optimize the filler content and crosshead speed. A second order mathematical model has been developed and the predicted optimum input parameters are 0.3 wt % Al_2O_3, 0.15 wt %TiO_2, and 500 mm/min crosshead speed. Furthermore, the model predicted results are compared with experimental one and found a close agreement between them. © 2016 Wiley Periodicals, Inc. J. Appl. Polym. Sci. **2016**, *133*, 44274.

KEYWORDS: dynamic mechanical thermal analysis; nano Al_2O_3 and TiO_2; response surface methodology; scanning electron micrograph; shear strength

Received 18 May 2016; accepted 4 August 2016

DOI: 10.1002/app.44274

INTRODUCTION

Fiber reinforced polymer (FRP) composites are becoming better alternative materials in different fields such as aerospace, automotive, marine, and so forth. due to its well-known advantage like high specific strength, performance, structural integrity in harsh and hostile environment as compared to that of traditional materials.[1] However, the interface/interphase is the weakest portion of FRP composites, which leads to early failure of the composite structure in transverse loading conditions. This is because; matrix transfers the load to strong fiber through the fiber/matrix interface/interphase. Hence, the interfacial strength is very critical and directly related to the strength and toughness of the composites.[2] Interface strength of the composites can be tailored through interlaminar shear strength (ILSS) and evaluated by short beam shear (SBS) test. It was observed that crosshead speed (CS) is sensitive to ILSS in FRP composites and the sensitivities persist in different environmental conditions. It was observed that hygrothermally conditioned glass fiber (GF) reinforced polymer (GFRP) composite is sensitive to CS and greater shear strength was observed at higher CS.[3] FRP composites subjected to ultra low temperature conditioning are also sensitive to CS.[4] It was also reported that ultra-low freezing and thawing,[5] thermal shocked,[6] subzero temperature treated[7] and at different environmental condition,[8,9] GFRP composites are sensitive to CS and ILSS increases with an increase in it.

Improvement of the ILSS of FRP composites is a major challenge for materials engineers/researchers to satisfy the design requirements in different structural applications subjected to transverse load. In such cases, impingement of nano fillers into the epoxy matrix is one of the methods to improve the mechanical properties of nano composites.[10,11] However, the improvement depends on the nano fillers concentration, shape, size, and interlink between the matrix, fiber and nano fillers. Broadly nano fillers are carbon based (CNT, SWCNT, MWCNT, and graphene), inorganic (SiO_2, SiC, etc.), metal (Fe, Al, etc.), metal oxide (TiO_2, Al_2O_3, ZnO, etc.) and others (WS_2, MoS_2 nano clay, etc.).[12] Addition of nano fillers into the polymer matrix composites enhances the mechanical properties, thermal stability and lowers the permeability as compared to that of neat epoxy GFRP composites.[13,14] Among different nano fillers, nano TiO_2 and Al_2O_3 are the most promising metal oxide fillers, because of their excellent mechanical, thermal, weathering properties, low density and low manufacturing cost as compared to carbon base nano fillers.[15–17]

Jiang *et al.*[18] found that at low content of nano Al_2O_3 improves glass transition temperature (T_g) by 11 °C and at higher content of Al_2O_3, both T_g and coefficient of thermal expansion decreases. Omrani and Rostami[19] found that flexural strength increases with increase in concentration of nano Al_2O_3. Wetzel *et al.*[20] observed that nano Al_2O_3 and $CaSiO_3$ improved stiffness and wear resistance of polymer composites. Zhao *et al.*[21] found that improvement of mechanical properties of nano composites is attributed to the enhancement of micro crack deflection as compared to without nano fillers. Blending of nano TiO_2 with epoxy improved the mechanical properties compared to neat epoxy composites.[22,23] The improvement of mechanical/thermal properties through nano inorganic or metal oxide particles may be attributed to good dispersion of nano particle leads to physicochemical/adhesive/van der Walls bond improvement and possible electrostatic interaction takes place with epoxy matrix.[24,25] Phasapan and Jantrawan[26] observed that silane treated nano TiO_2 improves the fracture toughness as well as impact strength. Nano particles also act as a strong stress concentration zone, which resist crack propagation, by which the strength of the nano composites was improved.[27]

Different researchers have found that individually either nano Al_2O_3 or TiO_2 has positive responses on mechanical properties. However, the combined effect of both nano particles at different wt % on physical and mechanical properties might be interesting and yet to be investigated. The effect of CS on the ILSS of this type of new nano-composites is still quite complex phenomenon. Therefore, the statistical tool is necessary to understand the interaction effect of both nano fillers on mechanical properties at different CS. Because, statistical tools have the capability to design, model, and optimize the input parameters and corresponding responses of nano fillers filled GFRP nanocomposites. In full factorial design, no of set of experiments is more, because it includes all possible interaction between the input parameters.[28] For instance, in a full factorial design of experiment, three input parameters with three levels need 27 no of experiments. However, only 15 no of experiments are needed in a Box–Behnken design of experiment of response surface methodology (RSM). RSM gives similar information like that of full factorial design with less nos of experiments.[28,29] Daneshpayeh *et al.*[15] have studied the mechanical properties of polypropylene (PP)/LLDPE/TiO2 ternary nano-composite system by RSM. It was observed that multioptimization statistical tool is very much helpful to predict the influence of significant input parameters on the mechanical properties of ternary nanocomposites. Rostamiyan *et al.*[30] evaluated the tensile and impact strength of epoxy/GF/SiO_2/clay hybrid composites using central composites design, which is a subset of RSM. Mirmohseni and Zavareh[31] studied the mechanical properties of quaternary nano composites using Taguchi design of experiment.

Therefore, the objective of this article is to study the combined effect of nano Al_2O_3 and TiO_2 content and CS on ILSS and predict the optimum combination of input parameters and its corresponding responses using RSM design of experiment. In the present investigation, Box–Behnken design of experiment is used to design, optimize and predict the input parameters and corresponding responses. Furthermore, the confirmation test has been conducted with optimized input parameters. Additionally, dynamic mechanical thermal analysis (DMTA) has been carried out to compare the glass transition temperature, elastic and viscoelastic modulus between nano and neat epoxy GFRP composites. Furthermore, evaluation of modes of failure has been studied through scanning electron microscopy (SEM) microscopic features observation.

EXPERIMENTAL

Materials and Sample Preparation

In the present investigation epoxy (Diglycidyl ether of Bisphenol A), hardener (Triethylene tetra amine, nano-fillers (Al_2O_3 and TiO_2), and woven roving GF (Warp and weft density: 6.3 and 5.5 threads/cm, respectively, Fabric weight: 360 gsm) are used as raw materials to fabricate the control and nano GF composites. Weight fraction of GF and epoxy is in the ratio of 60:40 approximately. Figure 1 shows the schematic view of the fabrication of nano GFRP composites. Initially nano Al_2O_3 and TiO_2 particles are dried at 100 °C for 2 h before mixing with the epoxy. Nano fillers are dispersed with epoxy using magnetic stirrer (70 °C, 1200 rpm) for 45 min and sonication (40 KHz) for about 60 min. Both control and nano GF composites are fabricated using hand lay-up technique and hot press molding at 10 kg/cm^2 molding pressure to reduce entrapped gases during mixing. Further curing is done at 140 °C for 6 h before characterization. Specimens are prepared for ILSS and DMTA test as per the ASTM standards. Table I indicates different type of composites fabricated and their compositions.

Characterization

Nano fillers compositions are characterized by X-ray diffraction (XRD) with Broker D8 advance XRD system. Co Kα source and a Lynxeye 1D detector are used in the XRD system. Figure 2(a,b) shows the XRD patterns of nano Al_2O_3 and TiO_2 fillers, respectively. From the intensity versus 2θ plot, it is observed that all the peaks comprises only Al_2O_3 and TiO_2, indicating good purity of commercial nano fillers.

Nano particle size plays an important role in its distribution in epoxy matrix. Particle size distribution of nano Al_2O_3 and TiO_2 has been analyzed by dynamic light scattering (DLC, Malvern) equipment. Nano particles are dispersed in alcohol and water (50:50 ratios) and followed by sonication before testing in DLC. It is observed that Z-average (d.nm) of nano Al_2O_3 and TiO_2 particles are 917 and 380 d.nm, respectively. The average nano particle size of TiO_2 is smaller than Al_2O_3. Therefore, it is expected that the probability of agglomeration of TiO_2 nano particles will be more as compared to nano Al_2O_3 particles in polymer-based nano composite. This is because of a reduction in the inter-particle distance at higher concentration of nano TiO_2 in an epoxy matrix.[32]

Figure 3 shows field emission scanning electron microscopy (FESEM) images of nano Al_2O_3 and TiO_2 distribution in epoxy matrix of nano composite (GF-I). Well dispersion of nano particles is observed in some places of developed composites. SBS test is performed to evaluate the apparent ILSS of the composites. ILSS is evaluated using Instron-5967 UTM machine at different CS by adjusting the crosshead velocity. The test is

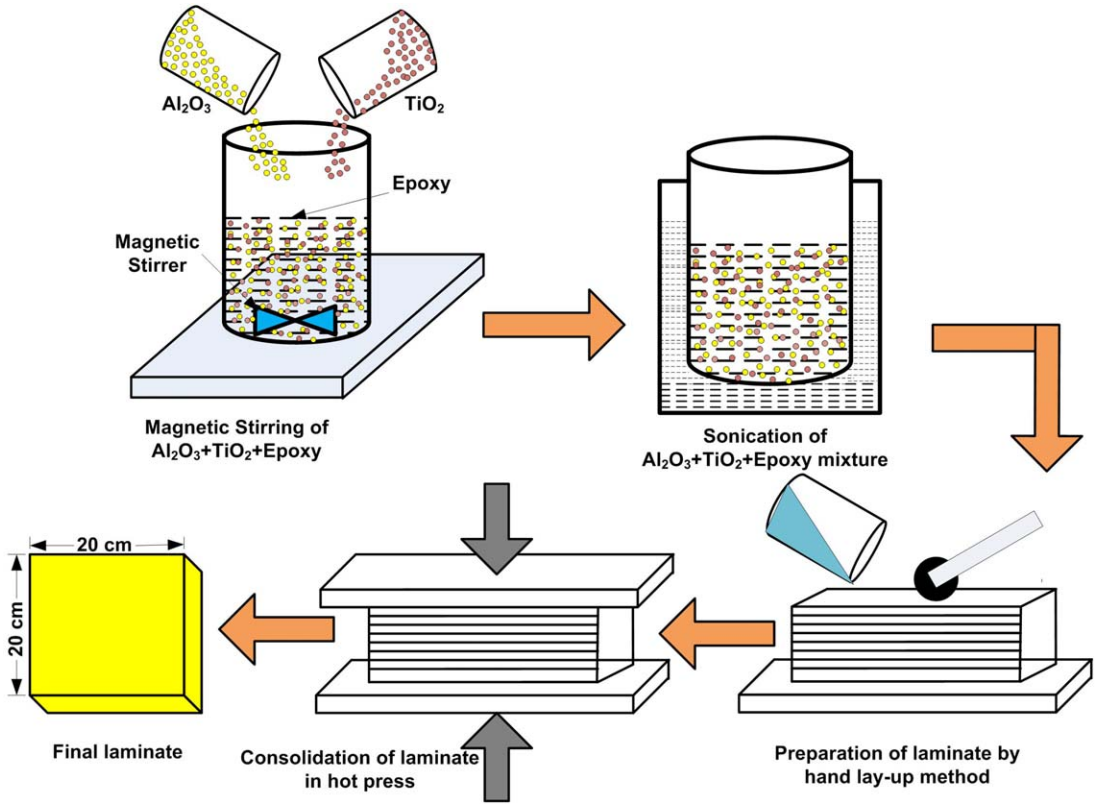

Figure 1. Schematic view of the fabrication of nano Al_2O_3 and TiO_2 filled GFRP composite laminates. [Color figure can be viewed in the online issue, which is available at wileyonlinelibrary.com.]

Table I. Different Composites and Their Composition

Fillers type	Symbol	Control GF	GF-A	GF-B	GF-C	GF-D	GF-E	GF-F	GF-G	GF-H	GF-I
Al_2O_3 wt %	*A*	0	0.1	0.1	0.1	0.3	0.3	0.3	0.7	0.7	0.7
TiO_2 wt %	*T*	0	0.1	0.3	0.7	0.1	0.3	0.7	0.1	0.3	0.7

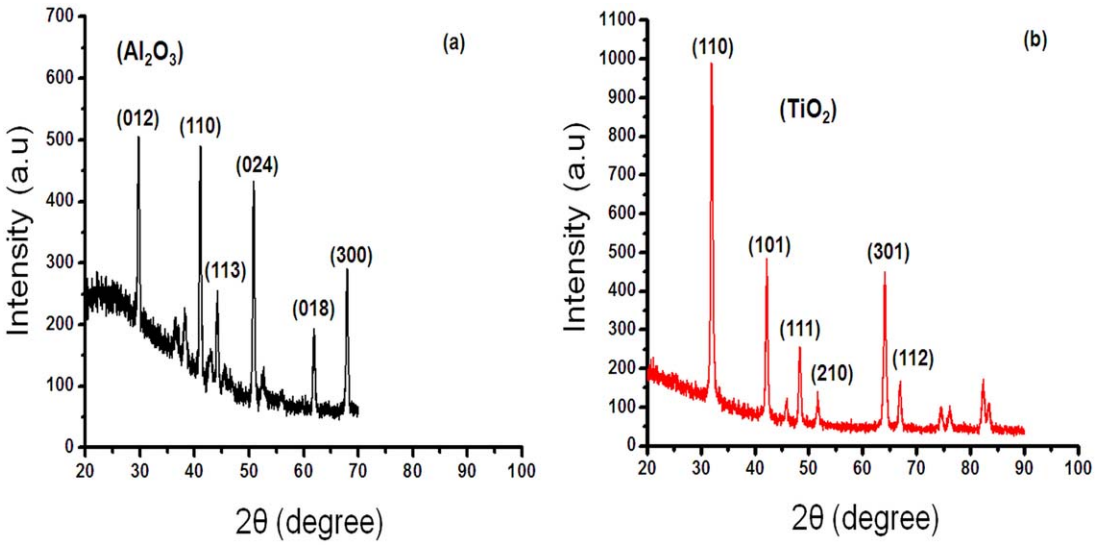

Figure 2. (a) Intensity versus 2-theta of (a) Al_2O_3 (b) TiO_2. [Color figure can be viewed in the online issue, which is available at wileyonlinelibrary.com.]

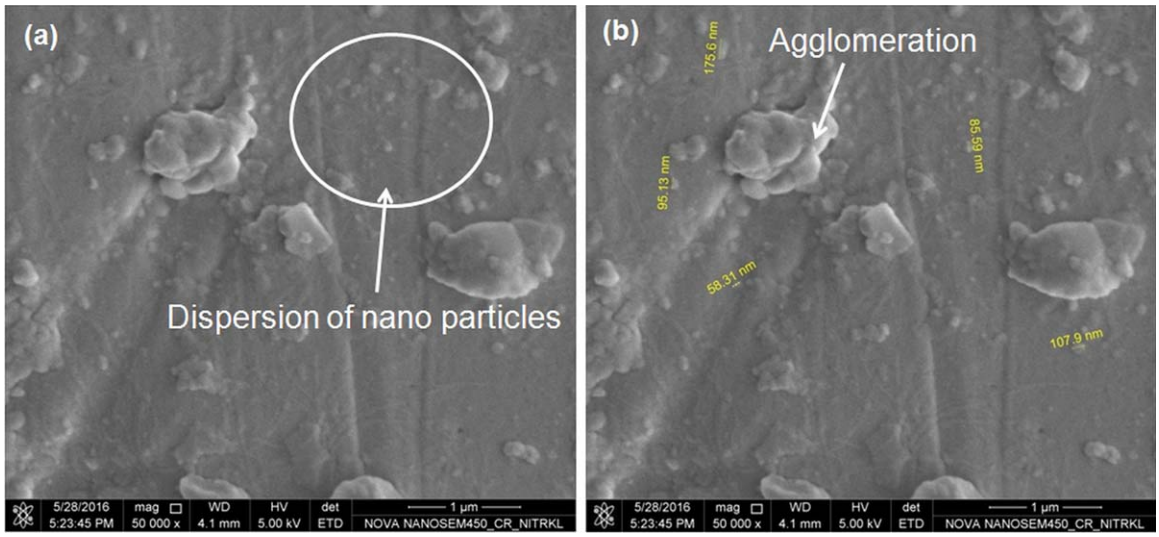

Figure 3. FE-SEM images of (a) nano particle distribution and (b) size of the nano particles in the epoxy matrix of the composites having $Al_2O_3 = 0.7$ wt % and $TiO_2 = 0.7$ wt %. [Color figure can be viewed in the online issue, which is available at wileyonlinelibrary.com.]

conducted as per the ASTM: D2344-13 standard. The sample size used for the test is 37 × 9 × 4.5 mm^3 and span length of 27 mm are maintained throughout the test. In three point bend test, the samples are placed in between two supporting rollers of 3-mm diameter and load is applied at the middle of the sample by another 6-mm diameter roller. At each CS minimum six samples are tested and the average values are reported. The specimens are tested at room temperature and at different CSs. The ILSS is calculated as per the eq. (1).

$$\text{ILSS} = \frac{3P}{4bt} \tag{1}$$

where P is the maximum load applied (N), t is the thickness (mm) and b is the width (mm) of the sample.

The elastic, viscoelastic, and thermal properties of the nano composites are studied using DMTA. The DMTA evaluation is performed using Netzsch DMA 242E equipment as per D7028 standard. In a perfectly elastic material, the stress and strain are in phase of dynamic loading condition. However, in viscoelastic material, the stress and strain are not in phase. DMTA analysis gives storage/elastic modulus (E') and loss/viscous modulus (E'') of a material as a function of temperature. The damping property of the material is evaluated from the parameter $\tan\delta$, which is the ratio of E'' to E'. Thermal properties also evaluated from $\tan\delta$. As epoxy/GF composites are viscoelastic material, hence DMTA analysis is done to compare the elastic, storage and glass transition temperature between nano and control GF composites [eqs. (2–4)].

$$E' = \frac{\sigma_0}{\varepsilon_0}\cos\delta \tag{2}$$

$$E'' = \frac{\sigma_0}{\varepsilon_0}\sin\delta \tag{3}$$

$$\tan\delta = \frac{E''}{E'} \tag{4}$$

where, σ_0 and ε_0 is the peak stress and strain, respectively, and δ is the phase difference between the stress and strain. The propagation of cracks and mode of failure of the fracture surfaces of ILSS samples is investigated by SEM and FESEM.

RESULTS AND DISCUSSION

Effect of Nano-Fillers on ILSS

ILSS has been evaluated at 1 mm/min CS by short-beam shear stress test and compared between control and nano GF composites. The compositions of control and nano GF composites are reported in Table I. ILSS at different CS is reported in Table II. It is observed that addition of nano Al_2O_3 and TiO_2 enhances the ILSS and strain as compared to control GF composite. This improvement of ILSS may be attributed to better interface/interphase bond between epoxy matrix and GF with the addition of nano fillers. However, with the increase in nano Al_2O_3 and TiO_2 concentration, ILSS decreases and this may be due to the agglomeration of nano particles as shown in Figure 3. This is because of reduction of effective surface area of nano particles/epoxy/fiber interface with increase in nano fillers concentration.[32–34] Huang *et al.*[35] found that the addition of organoclay in the immiscible blend of PP and polyamide (PA6), tensile strength increases initially and declines dramatically with further increase in organoclay content even though percolated clay network was observed.

Effect of CS on ILSS

ILSS has been evaluated for control and nano GF composites at different CS. Maximum ILSS and strain at different CS are highlighted in Table II. It is observed that ILSS increases with an increase in CS up to 100 mm/min and decreases with further increases in CS. The results revealed that at higher concentration of nano TiO_2, keeping nano Al_2O_3 at a lower level, ILSS decreases and it may be due to the agglomeration of nano TiO_2 particles. As the average particle size of nano TiO_2 particles is smaller than nano Al_2O_3, smaller particles reduces the interparticle distance and enhanced the agglomeration tendency.[29] The increase or decrease in ILSS with CS are attributed to increase in stiffness of the composites and brittle behavior of the matrix, respectively. Similar behavior has also observed by

Table II. Interlaminar Shear Strength (ILSS) and Strain at Different Crosshead Speed

		Crosshead speed (CS; mm/min)				
Composites types	Properties	1	50	100	500	1000
Control GF	ILSS (MPa)	26.55	29.90	32.28	30.46	27.00
	Strain (%)	2.9	3.1	3.1	4.3	4.6
GF-A	ILSS (MPa)	**31.63**	**32.76**	**35.00**	31.77	31.44
	Strain (%)	3.2	3.2	2.8	3.8	4.5
GF-B	ILSS (MPa)	28.00	29.69	30.72	28.45	28.00
	Strain (%)	2.6	3.2	3.3	4.0	4.1
GF-C	ILSS (MPa)	23.13	25.46	26.00	24.71	24.62
	Strain (%)	2.5	2.8	3.1	3.4	4.1
GF-D	ILSS (MPa)	30.00	31.97	33.29	32.62	31.00
	Strain (%)	3.0	3.2	3.4	4.3	4.5
GF-E	ILSS (MPa)	27.83	28.22	28.00	27.56	27.00
	Strain (%)	2.7	3.9	3.72	**4.5**	**4.7**
GF-F	ILSS (MPa)	25.00	26.63	27.51	26.51	25.00
	Strain (%)	**3.4**	**3.7**	**4.1**	4.2	4.4
GF-G	ILSS (MPa)	28.47	32.00	33.00	29.48	29.17
	Strain (%)	2.7	3.0	3.3	3.7	4.3
GF-H	ILSS (MPa)	30.00	32.52	34.51	31.51	30.00
	Strain (%)	2.9	3.1	3.2	3.8	4.3
GF-I	ILSS (MPa)	30.32	32.17	**35.00**	**33.53**	**31.50**
	Strain (%)	2.9	3.4	3.5	3.9	**4.7**

Sethi *et al.*[36] in GF composites. The decreases or increase in ILSS may be due to the following reasons (i) at a lower CS some micro-cracks turn into potential cracks and cause a significant reduction in ILSS (ii) the interface integrity improves because of longer relaxation time. At higher CS, plastic deformation zone may be formed ahead of the crack tip because of matrix deformation. In the meantime fiber can pull out from the matrix behind the crack tip. As fiber pull out is energy absorbing mechanism, at a higher CS, ILSS reduces. It is also observed that shear stain increases with an increase in CS irrespective of nano filler type and their concentration.

From the experimental results reported in Table II, it is difficult to suggest a particular composite type and CS at which maximum ILSS and strain can be achieved. Therefore, in the present study RSM is used for modeling and optimization of nano filler type, concentration, and CS to achieve maximum ILSS and strain.

Effect of Nano Fillers on Loss and Storage Modulus

DMTA analysis has been conducted for control and nano GF composites. The analysis has been done at a frequency of 1Hz, temperature range from 40 to 200 °C, heating rate of 10 °C/min and 3 point bending mode. Figure 4(a–c) shows the variation of storage modulus, loss modulus and tan δ as a function of temperature, respectively. It is observed that storage modulus is reduced with an increase in nano Al_2O_3 content. Jiang *et al.*[18] has also observed the similar effect. This may be attributed to an increase in wt % of nano Al_2O_3 particle, increases the hindrance in crystallinity of nano composites because of agglomeration of nano particles. Furthermore, the agglomerated nano particles reduce the probability to enter into the interchain spacing of polymer, leading to decrease in crosslink formation between polymer and nano particles. However, the glass transition temperature does not have much effect with the change in nano particles wt %, which is observed from tan δ versus temperature plot. The glass transition temperature is around 140 °C for both types of composites. This indicates TiO_2 and Al_2O_3 do not have an influence on the stability of the epoxy polymer matrix at high temperature. Daneshpayeh *et al.*[15] also found that the glass transition temperature has not been changed with the addition of nano TiO_2 in PP/LLDPE polymer nano composites. Jiang *et al.*[18] has also observed that with increase in nano Al_2O_3 wt %, glass transition temperature was not changed in epoxy resins/nano-Al_2O_3 composites.

Evaluation of Failure Modes through Microscopic Features Analysis

The mode of failure at different CS and the strengthening mechanism of the nano composites have been investigated through SEM and field emission SEM. Figure 5 shows the dominated fracture mode in (a) low and (b) high CS for control GF composite. Figure 6 shows the failure mechanism of the nano GF-A composite at (a) low and (b) high CS. It is observed that at lower CS, crack initiated at the fiber-matrix interface and propagate through weak matrix. However, at high CS fiber-matrix interface failure is the dominating mechanism for the failure of the composites. A similar observation was reported by Ray *et al.*[37] and Rahman *et al.*[38]

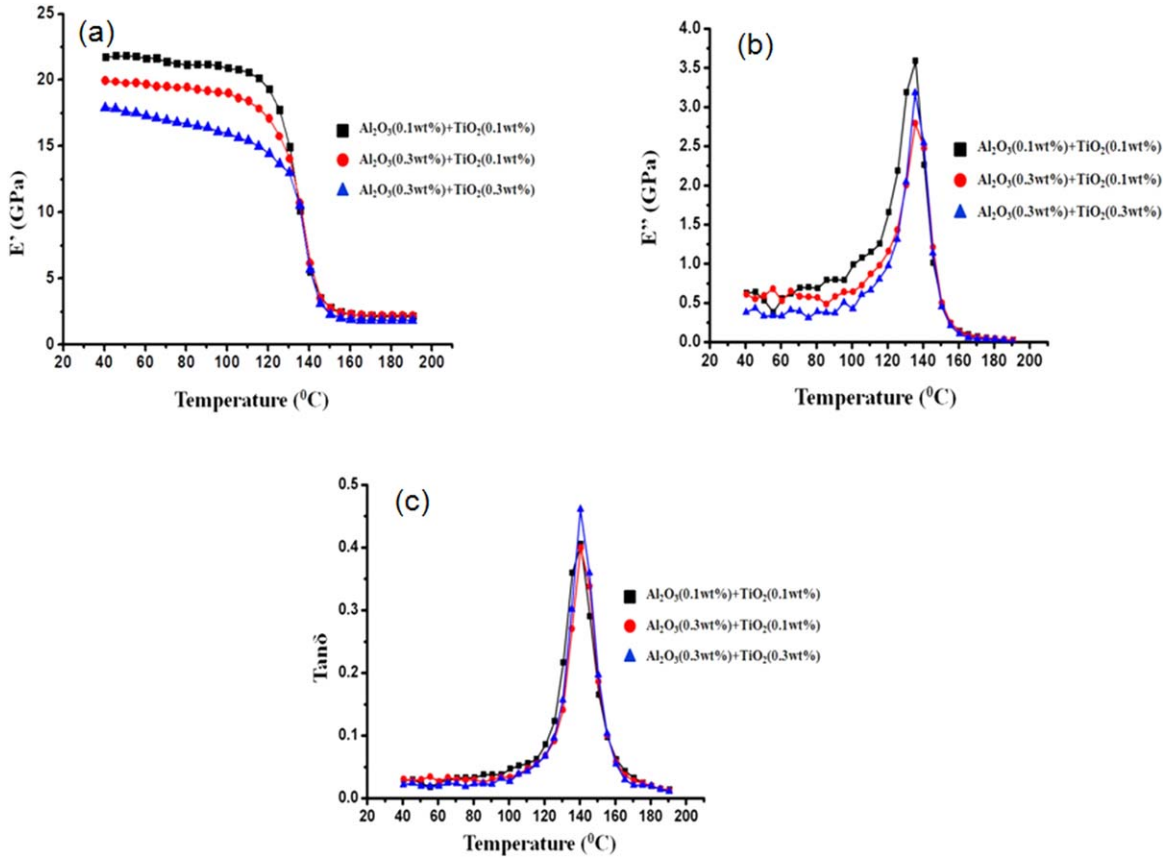

Figure 4. (a) storage modulus (E') (b) loss modulus (E''), and (c) tan δ as a function of temperature. [Color figure can be viewed in the online issue, which is available at wileyonlinelibrary.com.]

Figure 7(a,b) indicates different failure modes at different CS. It is observed that at lower CS the mode of fracture was the combination of interfacial debonding, fiber pull out and fiber breakage. However, at the high CS, the mode of failure is the combination of fiber pullout and interfacial debonding. Figure 8(a) shows fracture surface of control GF composite and (b) Nano GF-A and (c) Nano GF-I composites. It is observed that in nano GF composite, the epoxy has zigzag dispersion and adhesion to the fiber surface. However, smooth fiber imprints are observed in control GF composites. Therefore, in nano GF composite the fracture surface areas increase as compared to control GF composite resulting improvement of ILSS of the nano composites. This may be because of nano

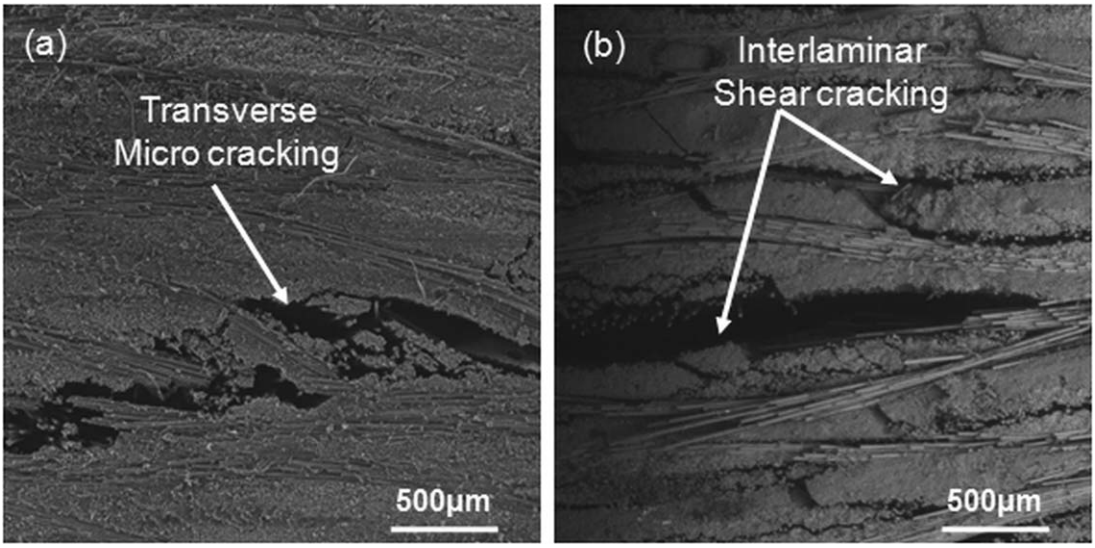

Figure 5. SEM image of failure modes of control GF sample (a) crosshead speed = 1 mm/min (b) crosshead speed = 1000 mm/min.

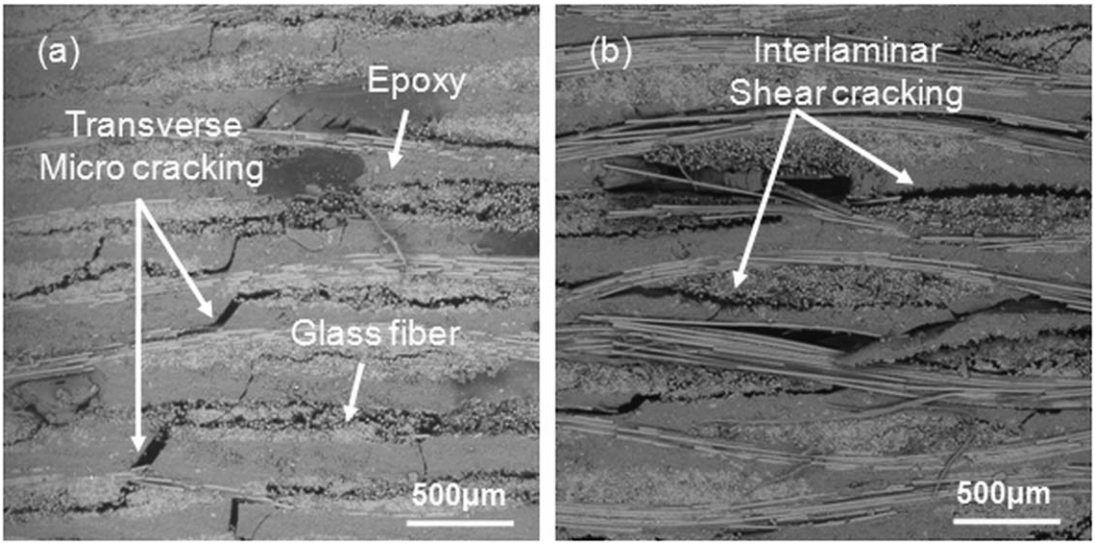

Figure 6. SEM image of failure modes of GF-A sample (a) crosshead speed = 1 mm/min (b) crosshead speed = 1000 mm/min.

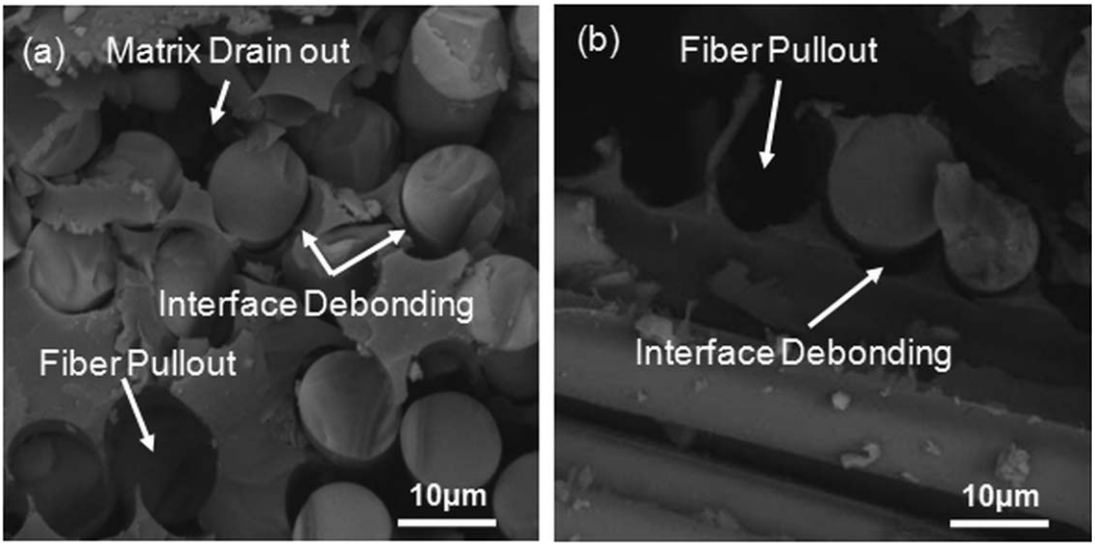

Figure 7. SEM image of the fracture surface for GF-A sample at (a) crosshead speed = 1 mm/min (b) crosshead speed = 1000 mm/min.

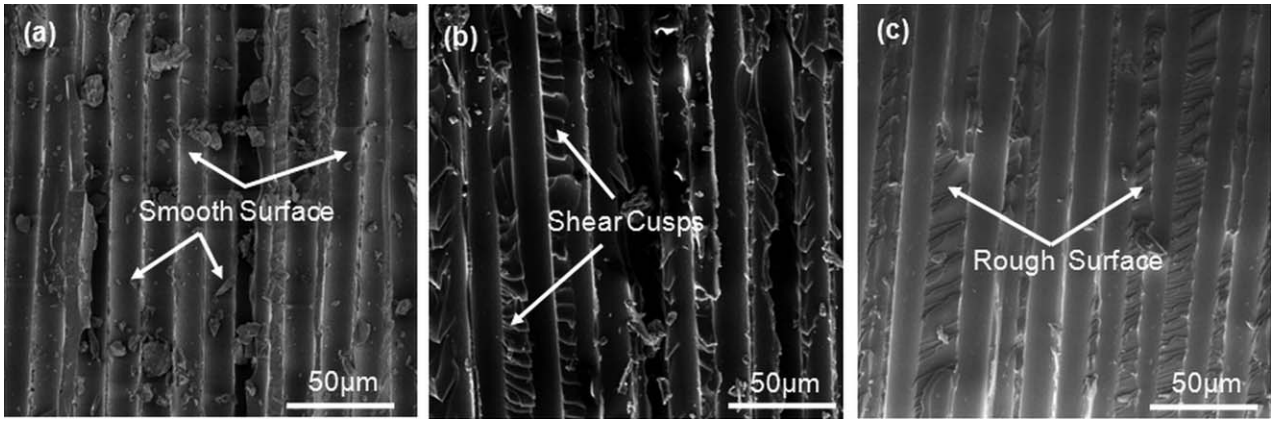

Figure 8. Field emission scanning electron microscopy images of the fractured surface feature of (a) control GF (b) GF-A (c) GF-I.

Table III. Factors and Their Levels in Box–Behnken Design of Experiment

Parameters	Symbol	Levels used		
		Low (−1)	Middle(0)	High(+1)
Al_2O_3 (wt %)	*A*	0.1	0.3	0.7
TiO_2 (wt %)	*T*	0.1	0.3	0.7
Crosshead speed (mm/min)	CS	1	100	1000

Al_2O_3 and TiO_2 particles prevented the micro crack growth and detoured it.[39]

From mechanical properties and microscopic observation, it is found that nano Al_2O_3 and TiO_2 content has the influence on the improvement and as well as degradation of mechanical properties. However, it is difficult to conclude at this point of time the best combination of nano filler content and CS at which maximum ILSS and strain can be obtained. Therefore, there is an urge to use a statistical tool to optimize the input parameters and their level to maximize the responses. RSM design of experiment has been adopted to find the optimum input parameters, their level to achieve maximum ILSS and strain.

Response Surface Methodology

Design of Experiment. A design of experiment is performed using Box–Behnken RSM for modeling and optimization of input parameters (Al_2O_3, TiO_2, and CS) and its responses (ILSS and strain). The statistical software Minitab17 is used to create and analyze the design matrix. Al_2O_3 (*A*), TiO_2 (*T*), and CS are chosen as the input parameters and known as factors. There are three levels of each factor has been considered and reported in Table III. As per the Box–Behnken design of the experiment, 15 numbers of experimental runs are performed, including three center points as reported in Table IV. In this study the experiments are randomly chosen to minimize the error arising from the experimental process. A polynomial model has been considered to correlate the relationship between the independent variables and response as expressed in eq. (5).

$$R=\alpha_0+\alpha_1 V_1+\alpha_2 V_2+\alpha_3 V_3+\alpha_{11} V_1^2+\alpha_{22} V_2^2 +\alpha_{33} V_3{}^2+\alpha_{12} V_1 V_2+\alpha_{13} V_1 V_3+\alpha_{23} V_2 V_3 \quad (5)$$

where R = response, V_1, V_2, and V_3 = input variables (*A*, *T*, and CS), α_0 = constant, α_1, α_2, and α_3 = the coefficient of polynomial for linear effect, α_{11}, α_{33} = coefficient of quadratic effect, and α_{12}, α_{13}, and α_{23} = coefficient of the polynomial for interaction effect.

Modeling and Optimization of ILSS. Analysis of variance (ANOVA) is a statistical method which draws a set of conclusion based on experimental data. To find the significant factor(s) contributing for the improvement of ILSS, ANOVA is performed. In ANOVA table, sum of squares (SS) estimate the Fishers variance ratio (*F*-value), which indicates the variation of the data from the mean value. The effects of the parameters are statistically significant when the P-value is less than 0.05.[28] The ANOVA analysis results of ILSS are reported in Table V. The values for the degree of freedom (DF), adjusted sum of squares (**AdjSS**), adjusted sum of mean squares (**AdjMS**), Fishers value (*F*), and probability value (*P*) for the response ILSS is mentioned in Table V. It is observed that *R*-square is close to 100% and it means the model is more valid and in good agreement with the experimental data. The high value of R^2adj (98.81%) and R^2pred (91.49%) indicate that the model has very good predictability. The coefficient of second-order polynomial is calculated by multiple regression analysis and it is based on ANOVA analysis. The quadratic model is expressed in eq. (6).

Table IV. Box–Behnken Experimental Design in Uncoded Form

Experimental run	*A*	*T*	CS	ILSS (MPa)	Strain (%)
1	0.1	0.3	1000	28	4.1
2	0.3	0.3	100	28	3.72
3	0.7	0.7	100	35	3.5
4	0.3	0.7	1000	25	4.4
5	0.1	0.1	100	35	2.8
6	0.3	0.1	1000	31	4.5
7	0.3	0.7	1	25	3.4
8	0.7	0.1	100	33	3.3
9	0.7	0.3	1000	30	4.3
10	0.3	0.3	100	27.5	3.68
11	0.1	0.7	100	26	3.1
12	0.7	0.3	1	30	2.9
13	0.3	0.1	1	30	3
14	0.1	0.3	1	28	2.6
15	0.3	0.3	100	28.3	3.7

Table V. ANOVA Results for ILSS

Source	DF	AdjSS	Adj MS	*F*-value	*P*-value
Model	9	139.608	15.512	130.150	0.00
Linear	3	70.154	23.385	196.200	0.00
A	1	22.233	22.233	186.540	0.00
T	1	43.444	43.445	364.510	0.00
CS	1	7.257	7.257	60.880	0.00
Square	3	45.228	15.076	126.490	0.00
A^2	1	18.386	18.386	154.260	0.00
T^2	1	18.119	18.119	152.020	0.00
CS^2	1	7.887	7.887	66.170	0.00
2-Way interaction	3	33.481	11.160	93.640	0.00
$A \times T$	1	32.011	32.011	268.580	0.00
$A \times CS$	1	0.000	0.000	0.000	0.96
$T \times CS$	1	0.173	0.173	1.450	0.28
Error	5	0.596	0.119		
Lack-of-fit	3	0.269	0.090	0.550	0.70
Pure error	2	0.327	0.163		
Total	14	140.204			

R^2 = 99.57% R^2(adj) = 98.81% R^2(pred) = 91.49%

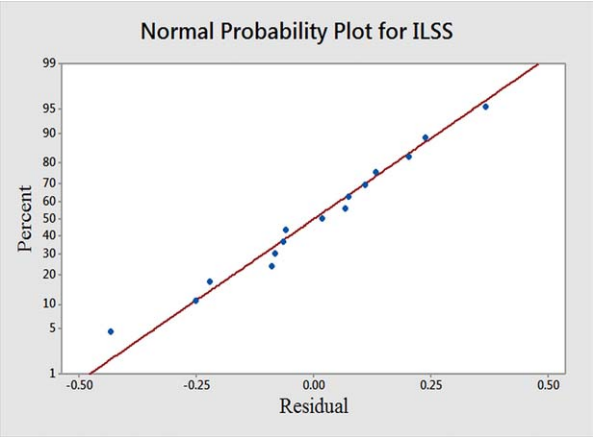

Figure 9. Normal probability plot of the residuals for ILSS. [Color figure can be viewed in the online issue, which is available at wileyonlinelibrary.com.]

$$\begin{aligned}\text{ILSS} = {} & 39.211 - 29.01A - 40.55T + 0.01936\text{CS} + 28.76A^2 \\ & + 28.55T^2 - 0.000019\text{CS}^2 + 30.19A^*T \\ & + 0.000052A^*\text{CS} - 0.001191\text{CS}\end{aligned} \quad (6)$$

In this quadratic equation, a positive sign in front of the coefficient indicates a synergistic effect and a negative sign indicates an antagonistic effect to ILSS. Among all the significant variables, CS has more contribution for the improvement of ILSS as compared to Al_2O_3 and TiO_2.

Figure 9 shows the normal probability plot for ILSS, where the residuals are near to the straight line and indicates the experimental data is normally distributed. Hence, it is safe to say that the data are reliable and the population of experimental data is normally distributed.

Figure 10 shows the main effect plot for ILSS. Here, the mean of ILSS is represented in theY-axis and the factors changes from lower to the maximum of their level are in *X*-axis. It is observed that with the increase in wt % *A*, ILSS decreases. Similarly with an increase in wt % *T* ILSS decreases. However, with an increase in CS, ILSS increases up to 100 mm/min and further decreases with an increase in CS. Similar behavior has also been observed by Sethi *et al.*[36] in GF epoxy composites.

Equation (6) is used to construct the 3D surface plot for ILSS. The ILSS has varied with *A* and CS keeping *T* at mid value. In a polynomial model, when the interaction effect is insignificant to the response, then the surface plot will be a flat plane. However, when the interaction effect is significant, the response surface plot will become twisted.[15] The 3D surface plots for ILSS against $Al_2O_3(A)$, CS, and (TiO_2) *T* are represented in Figure 11(a,b), respectively.

Figure 11(a) shows a 3-D surface plot for ILSS, when TiO_2 is in mid value(0.3 wt %). It is observed that at low values of Al_2O_3 (0.1 wt %) and mid value of CS (500 mm/min), ILSS is maximized. From Figure 11(b), it is observed that low values of TiO_2 (0.1 wt %), mid value of CS (500 mm/min), and Al_2O_3 (0.3 wt %), ILSS is maximized. Hence, it may be concluded that the most significant factors and their levels at which maximum ILSS could be achieved are low value of Al_2O_3 and TiO_2 and mid value of CS. This may be reasonably explained that with the increase in nano Al_2O_3 and TiO_2 concentration, the probability of agglomeration of nano particles increases and in consequence decreases the ILSS. Similar observation also found by Daneshpayeh *et al.*[15] and Omrani and Rostami.[19]

Modeling and Optimization of Strain. Shear strain at peak load is determined from ILSS test. To determine the significant factor(s) contributing to improve the strain at peak load, ANOVA has been performed to find the significant parameters affecting strain in the nano-composites system. Table VI shows ANOVA analysis results for strain. From the ANOVA analysis, it is observed that *R*-square is close to 100% and it means the model is more valid and very good fitting with the experimental data. The high value of R^2adj (99.28%) and R^2pred (93.43%) indicate that the model has very good predictability.

Figure 12 shows the normal probability plot for strain, where the residuals are near to the straight line and indicates the data is normally distributed. Therefore, it is safe to say that the data is reliable and the data collected from the experiments are normally distributed. The coefficient of second-order polynomial is calculated by multiple regression analysis, which is based on ANOVA analysis. The quadratic model is expressed as follows:

$$\begin{aligned}\text{Strain} = {} & 1.6164 + 5.869\,A + 2.077\,T + 0.005191\,\text{CS} - 6.293\,A^2 \\ & - 1.761\,T^2 - 0.000003\,\text{CS}^2 - 0.276\,A^*T \\ & - 0.000376\,A^*\text{CS} - 0.000795\,T^*\text{CS}\end{aligned} \quad (7)$$

Among all the significant variables, $Al_2O_3(A)$, $TiO_2(T)$, and CS have the contribution to strain due to their positive linear coefficient. However, the coefficient of Al_2O_3 is more than TiO_2 and CS; hence, Al_2O_3 has more influence on strain than other parameters.

Figure 13 shows the main effect plot for strain. Here, the main effect is represented when the factors changed from the lower to the maximum of their level. It is observed that with increase in wt % Al_2O_3, strain increases. Previous researchers also observed that the tensile strain increases with Al_2O_3 nano fillers as compared to neat epoxy.[34] It is also observed that with the increases in CS strain increases. This may be because at high CS the

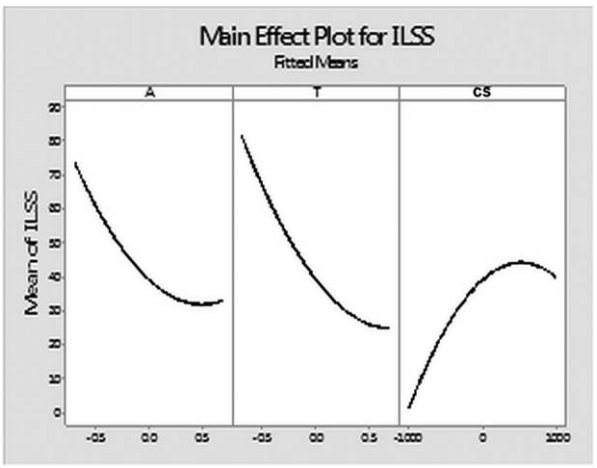

Figure 10. Main effect plot for ILSS.

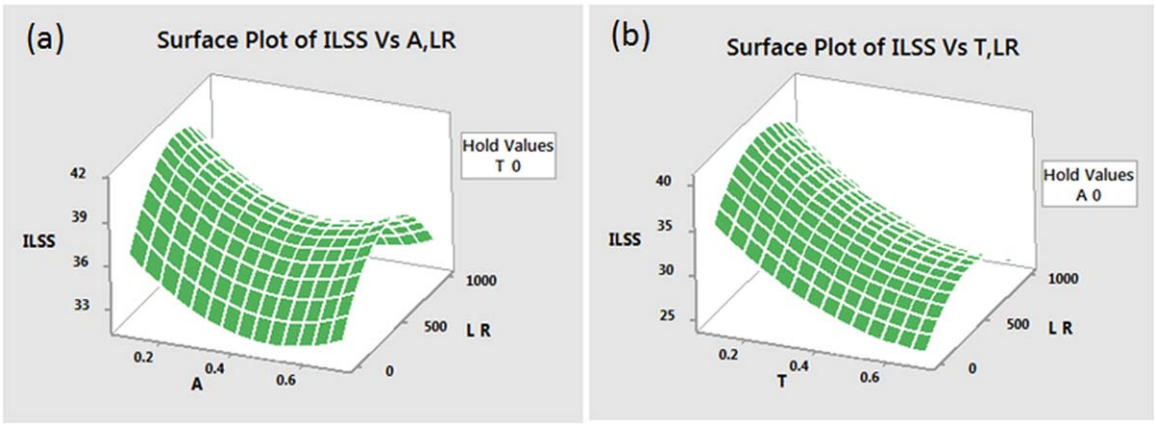

Figure 11. Three-dimensional surface plot of (a) ILSS versus *A* and CS and (b) ILSS versus *T* and CS. [Color figure can be viewed in the online issue, which is available at wileyonlinelibrary.com.]

micro-cracks may not find sufficient time to find the weakest path for fracture. Meantime, nano particles obstruct the movement of micro cracks in the composites because nano particles are tougher as compared to neat epoxy. Hence, the micro-cracks need to move either along the surface of the nano particle or cut the nano particle or crack may blunt at the nano particle. In this process, the composites requires more stress if the crack need to pass through the nano particles or blunt the crack if stress is not sufficient enough. If it will bypass or divert the path because of nano particle, then the micro crack needs to move more distance before fracture. During this process, the strain increases. Similarly, in case of TiO_2, with an increase in wt %TiO_2, strain increases. But the rate of increment is very low as compared to nano Al_2O_3. This may be reasonably attributed to aggregates of nano TiO_2 particles, because nano TiO_2 size is smaller as compared to nano Al_2O_3 particles. Hence, the probability of formation of nano TiO_2 aggregates is more than nano Al_2O_3.[32]

Table VI. ANOVA Results for Strain

Source	DF	Adj SS	Adj MS	*F*-value	*P*-value
Model	9	4.90418	0.544909	215.83	0.000
Linear	3	1.30542	0.43514	172.35	0.000
A	1	0.90983	0.909834	360.37	0.000
T	1	0.11398	0.113979	45.15	0.001
CS	1	0.52152	0.521523	206.57	0.000
Square	3	1.11711	0.37237	147.49	0.000
A^2	1	0.87992	0.879917	348.52	0.000
T^2	1	0.06889	0.068886	27.29	0.003
CS^2	1	0.26883	0.268827	106.48	0.000
2-Way interaction	3	0.09068	0.030226	11.97	0.010
$A \times T$	1	0.00268	0.002676	1.06	0.350
$A \times CS$	1	0.0172	0.017198	6.81	0.048
$T \times CS$	1	0.077	0.076996	30.5	0.003
Error	5	0.01262	0.002525		
Lack-of-fit	3	0.01182	0.003941	9.85	0.094
Pure error	2	0.0008	0.0004		
Total	14	4.9168			

$R^2 = 99.74\%$ $R^2(\text{adj}) = 99.28\%$ $R^2(\text{pred}) = 93.43\%$

Equation (7) is used to construct a 3D surface plot for strain. The strain is varied with *A* and CS keeping *T* at mid value. Figure 14(a) shows the graphical 3D surface plot for strain, when TiO_2 is in mid value ($T = 0.3$ wt %). It is observed that at mid value of Al_2O_3 (0.3 wt %) and high value of CS (1000 mm/min), strain is maximum. Figure 14(b) shows the graphical 3D surface plot for strain, when Al_2O_3 is in mid value ($A = 0.3$ wt %). It is observed that at mid value of TiO_2 (0.3 wt %) and high value of CS (1000 mm/min), strain is maximized. Hence, it may be concluded that the most significant factor and level for maximum strain is the mid value of Al_2O_3, mid value of TiO_2 and high value of CS. Nguyen *et al.*[40] observed that with the increase in TiO_2 content, elongation increase in LDPE/TiO_2 nano composites.

Prediction of Optimal Conditions. Optimization of RSM undergoes the following general steps.[15]

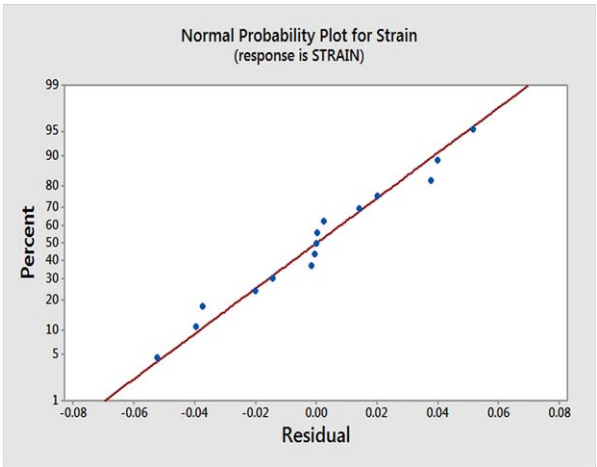

Figure 12. Normal probability plot of the residuals for strain. [Color figure can be viewed in the online issue, which is available at wileyonlinelibrary.com.]

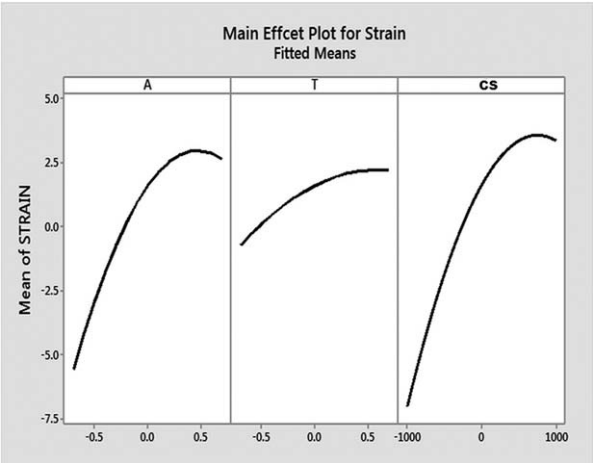

Figure 13. Main effect plot for strain.

1. Screening: The experiments are designed in such a way that the control parameters should have a statistically significant effect for the objective of the study.
2. Modeling: Experiments are designed in such a way that the response should be a function of control parameters.
3. Optimization: From the response model, optimum conditions of the control parameters need to be found out.

ILSS and strain at peak load are optimized simultaneously. Multiple response optimizations have been done using the desirability function. In this approach, the response model (R) will be converted into individual desirability functions (d) and that are again aggregated to a composite desirability function (D). The composite function is nothing but geometric or arithmetic mean, which need to be maximized or minimized, respectively. The individual desirability function varies in the range of $0 \leq d \leq 1$.

There are three types of desirability functions, which depend on the response characteristics.[41]

1. The higher is the better, that is, the objective function needs to be maximized.
2. The lower is the better, that is the objective function needs to be minimized.

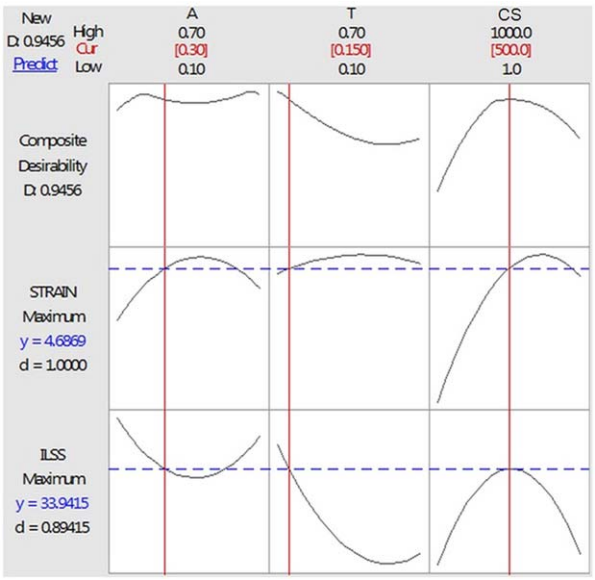

Figure 15. Desirability plot for multioptimization of responses. [Color figure can be viewed in the online issue, which is available at wileyonlinelibrary.com.]

3. The nominal is the best, that is, objective function needs to be achieved a particular target.

In this study, both the responses (i.e., ILSS and strain at peak load) need to be maximized. Therefore, the individual desirability function should be "higher is the better." The target is the response (R) should be maximized. Therefore, the individual desirability function could be defined as given in eq. (8):

$$d = \begin{cases} 0 & y < L \\ \left(\frac{R-L}{T-L}\right)^r & L \leq y \leq T \\ 1 & y > T \end{cases} \quad (8)$$

where L indicates the lower limit of the response, the characteristics of a desirability function(d) depends on the value r (weight).

If $r = 1$, then d is linear.

If $r > 1$, then d is near to the target value.

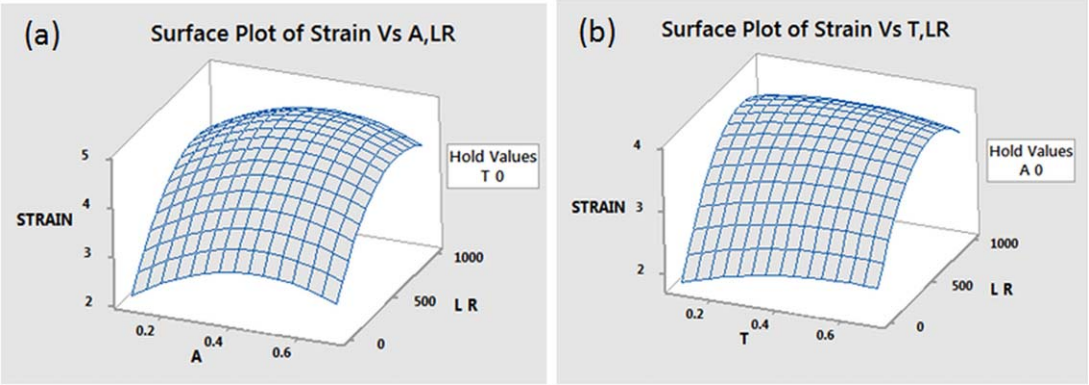

Figure 14. Three-dimensional surface plot of (a) strain versus Al_2O_3 and CS and (b) strain versus TiO_2 and LR. [Color figure can be viewed in the online issue, which is available at wileyonlinelibrary.com.]

Table VII. Results of Confirmation Experiment for Optimal Condition

Optimum values	Optimal parameters		Control GF composites (Reference)
	Prediction	Confirmation experiment	
Optimal values (wt %)	Al_2O_3 at 0.3 wt %	Al_2O_3 at 0.3 wt %	Al_2O_3 = 0.0 wt %
	TiO_2 at 0.15 wt %	TiO_2 at 0.15 wt %	TiO_2 = 0.0 wt %
	Crosshead speed at 500 mm/min	Crosshead speed at 500 mm/min	Crosshead speed at 500 mm/min
ILSS (MPa)	33.94	33.62	30.46
Strain (%)	4.68	4.62	4.3

If $0 < r < 1$, then d has less importance and far away from the target value.

In this study, we have to optimize two responses. Therefore, $r = 0.5$ is considered. For the ideal case the desirability function (d) =1. The composites desirability function $D(x)$ is computed by the geometric mean of the individual desirability functions d_i ($y_i(x)$) and given in eq. (9).

$$D(x) = [d_1(y_1(x)) \times d_2(y_2(x)) \times \ldots\ldots \times d_m(y_m(x))]^{1/m} \quad (9)$$

$$D = [d_1(\mathrm{ILSS}(x)) \times d_2(\mathrm{strain}(x))]^{1/2} \quad (10)$$

where m denotes the number of responses and in this model it is 2. As there are two responses are in this study, the composite desirability function is expressed in eq. (10). D denotes the composite desirability function, d_1 and d_2 are the individual desirability function corresponding to first and second responses (i.e., ILSS and strain), respectively. Here, the composite desirability function (D) needs to be maximized, that is, $D = 1$. This can be possible when all responses are on target, that is, $d_i = 1$. However, if $D = 0$, then one response is outside of the specification limit ($d_i = 0$ for any i). Otherwise the multiplicative d_i will yield a value which is less than or equal to the minimum value of d_i.

The optimization computation is performed by Minitab17 software and the results are shown in Figure 15. It is observed that to maximize the ILSS and strain simultaneously under maximum desirability ($D = 0.9456$), the parameter levels need to be set under the following conditions: Al_2O_3 at 0.3 wt %, TiO_2 at 0.15 wt %, and CS at 500 mm/min. In other words, the RSM model predicts the response using the above condition and found ILSS = 33.94 MPa and stain = 4.68 mm. It is observed that the composites desirability (0.9456) function is close to one. This means the setting parameters seem to be achieved favorable results for all responses. However, the individual desirability indicates that the setting parameters are more effective at maximizing the ILSS ($d = 0.894$) than the strain ($d = 1$).

Confirmation of Predicted Results

The RSM model predicts the optimum input parameters, their level and corresponding responses (ILSS and strain) for this design of experiment and reported in Table VII. The confirmation test is performed experimentally to verify the repeatability and reproducibility of the statistical method. The ILSS and strain obtained from the confirmation experiments are closely related to the data obtained in desirability optimization by RSM. The optimized ILSS and strain values are also compared with control GF composites and found improvement of ILSS and strain is about 10 and 7%, respectively.

CONCLUSIONS

The present investigation may lead to the following conclusions.

1. Addition of multiple nano fillers into the epoxy matrix has improved the ILSS about 16% at 0.1 wt % Al_2O_3 and 0.1 wt % TiO_2, 1 mm/min CS and shear strain about 24% at 0.3 wt % Al_2O_3 and 0.7 wt % TiO_2, 100 mm/min CS as compared to that of control GF composites.
2. ILSS and strain are sensitive to CS for both nano and control GF composites. However, the degree of sensitiveness is less in nano composites as compared to that of control GF composites.
3. DMTA analysis revealed that loss and storage modulus properties are deteriorated in nano GF composites as compared to control GF composites. However, there is no significant change in glass transition temperature.
4. Microscopic features revealed that, at lower CS matrix failure is the dominating failure mechanism and interface-failure is the possible dominating failure mechanism at higher CS.
5. From ANOVA, it is observed that all three parameters, that is, nano particles (Al_2O_3, TiO_2) and CS are significant variables for ILSS and strain in nano composites.
6. The RSM model predicted the optimum combination of input parameters at which maximum ILSS and strain can be achieved, that is, Al_2O_3 = 0.3 wt %, TiO_2 = 0.15% wt % and CS = 500 mm/min.
7. Using RSM models, desirability function was used for the multiresponse optimization. The optimized parameters for maximum ILSS and strain are predicted and those parameters are further validated by confirmation test and found the model predictability is very good agreement with experimental results.

ACKNOWLEDGMENTS

The authors are heartily thankful to KIIT University, Bhubaneswar, National Institute of Technology, Rourkela for providing infrastructural support for carrying out the present research work.

REFERENCES

1. Mangalgiri, P. D. *Bull. Mater. Sci.* **1999**, *22*, 657.
2. Dirand, X.; Hilaire, B.; Soulief, J. P.; Nardin, M. *Compos. Sci. Technol.* **1996**, *56*, 533.
3. Ray, B. C. *J. Reinf. Plast. Compos.* **2006**, *25*, 1227.
4. Ray, B. C. *J. Appl. Polym. Sci.* **2006**, *100*, 2289.
5. Ray, B. C. *J. Reinf. Plast. Compos.* **2005**, *24*, 1771.
6. Ray, B. C. *Mater. Lett.* **2004**, *58*, 2175.
7. Ray, B. C. *Mat. Sci. Eng. A* **2004**, *379*, 39.
8. Ray, B. C. *J. Reinf. Plast. Compos.* **2006**, *25*, 1227.
9. Ray, B. C. *Polym. Polym. Compos.* **2007**, *15*, 1.
10. Jongsomjit, B.; Chaichana, E.; Praserthdam, P. *J. Mater. Sci.* **2005**, *40*, 2043.
11. Dikobe, D. G.; Luyt, A. S. *Express Polym. Lett.* **2010**, *4*, 729.
12. Naffakh, M.; Díez-Pascual, A. M.; Marco, C.; Ellis, G. J.; Gómez-Fatou, M. A. *Prog. Polym. Sci.* **2013**, *38*, 1163.
13. Anjana, R.; George, K. E. *Int. J. Eng. Res. Appl.* **2012**, *4*, 868.
14. Garcia, M.; Vilet, G. V.; Jain, S. *Rev. Adv. Mater. Sci.* **2004**, *6*, 169.
15. Sajjad, D.; Faramarz, A. G.; Ismail, G.; Mohsen, A. *Compos. Part B Eng.* **2016**, *84*, 109.
16. Nayak, R. K.; Dash, A.; Ray, B. C. *Proc. Mater. Sci.* **2014**, *6*, 1359.
17. Sharifi Golru, S.; Attar, M. M.; Ramezanzadeh, B. *Prog. Org. Coat.* **2014**, *77*, 1391.
18. Jiang, W.; Jin, F.-L.; Park, S.-J. *J. Ind. Eng. Chem.* **2012**, *18*, 594.
19. Omrani, A.; Rostami, A. A. *Mater. Sci. Eng. A* **2009**, *517*, 185.
20. Wetzel, B.; Haupert, F.; Zhang, M. Q. *Compos. Sci. Technol.* **2003**, *63*, 2055.
21. Zhao, S.; Schadler, L. S.; Duncan, R.; Hillborg, H.; Auletta, T. *Compos. Sci. Technol.* **2008**, *68*, 2965.
22. Salehian, H.; Jahromi, S. A. J. *J. Compos. Mater.* **2015**, *49*, 2365.
23. Hamad, A.; Al-Turaif *Prog. Org. Coat.* **2010**, *69*, 241.
24. Zabihi, O.; Aghaie, M.; Zare, K. *J. Therm. Anal. Calorim.* **2013**, *111*, 703.
25. Basílio de Souza, J. P.; Laredo dos Reis, J. M. *Nanomater. Nanotechnol.* **2015**, *5*, 18.
26. Sanemuang, P.; Pumchusak, J. *Malays. J. Anal. Sci.* **2014**, *18*, 478.
27. Shi, G.; Qiu Zhang, M.; Rong, M. Z.; Wetzel, B.; Friedrich, K. *Wear* **2004**, *256*, 1072.
28. Montgomery, D. C. Design and Analysis of Experiments; Wiley: New York, **2001**.
29. Box, G. E. P.; Wilson, K. B. *J. R. Stat. Soc. B* **1951**, *13*, 105.
30. Rostamiyan, Y.; Fereidoon, A.; Mashhadzadeh, A. H.; Ashtiyani, M. R.; Salmankhani, A. *Compos. B Eng.* **2015**, *69*, 304.
31. Mirmohseni, A.; Zavareh, S. *Mater. Des.* **2010**, *31*, 2699.
32. Friedrich, K.; Fakirov, S.; Zhang, Z. Polymer Composites, from Nano- to Macroscale; Springer, **2005**.
33. Nielsen, L. E.; Landel, R. F. Mechanical Properties of Polymers and Composites; Marcel Dekker: New York, **1994**.
34. Asi, O. *Compos. Struct.* **2010**, *92*, 354.
35. Huang, J.; Zhu, Y.; Jiang, W.; Cardinaels, R.; Moldenaers, P.; Shi, D. *Int. Polym. Process.* **2014**, *29*, 4522.
36. Sethi, S.; Rathore, D. K.; Ray, B. C. *Mater. Des.* **2015**, *65*, 617.
37. Ray, B. C.; Rathore, D. *Crit. Rev. Solid State Mater. Sci.* **2015**, *40*, 119.
38. Rahman, M. M.; Zainuddin, S.; Hosur, M. V.; Robertson, C. J.; Kumar, A.; Trovillion, J.; Jeelani, S. *Compos. Struct.* **2013**, *95*, 213.
39. Wang, Z.; Huang, X.; Bai, L.; Du, R.; Liu, Y.; Zhang, Y.; Zhao, G. *Compos. Part B* **2016**, *91*, 392.
40. Nguyen, V. G.; Thai, H.; Mai, D. H.; Tran, H. T.; Tran, D. L.; Tuan Vu, M. *Compos. Part B Eng.* **2013**, *45*, 1192.
41. Kim, K.; Lin, D. *J. R. Stat. Soc. C Appl.* **2000**, *49*, 311.